AURORAL PLASMA ACCELERATION ABOVE MARTIAN MAGNETIC ANOMALIES

R. LUNDIN[1,*], D. WINNINGHAM[2], S. BARABASH[1], R. FRAHM[2], D. BRAIN[11],
H. NILSSON[1], M. HOLMSTRÖM[1], M. YAMAUCHI[1], J. R. SHARBER[2],
J.-A. SAUVAUD[3], A. FEDOROV[3], K. ASAMURA[4], H. HAYAKAWA[4], A. J. COATES[5],
Y. SOOBIAH[5], C. CURTIS[6], K. C. HSIEH[6], M. GRANDE[7], H. KOSKINEN[8],
E. KALLIO[8], J. KOZYRA[9], J. WOCH[10], M. FRAENZ[10], J. LUHMANN[11],
S. MCKENNA-LAWLER[12], S. ORSINI[13], P. BRANDT[14] and P. WURZ[15]

[1]*Swedish Institute of Space Physics, Box 812, S-98 128, Kiruna, Sweden*
[2]*Southwest Research Institute, San Antonio, TX 7228-0510, USA*
[3]*Centre d'Etude Spatiale des Rayonnements, BP-4346, F-31028 Toulouse, France*
[4]*Institute of Space and Astronautical Science, 3-1-1 Yoshinodai, Sagamichara, Japan*
[5]*Mullard Space Science Laboratory, University College London, Surrey RH5 6NT, UK*
[6]*University of Arizona, Tucson, AZ 85721, USA*
[7]*Rutherford Appleton Laboratory, Chilton, Didcot, Oxfordshire OX11 0QX, UK*
[8]*Finnish Meteorological Institute, Box 503 FIN-00101 Helsinki, Finland*
[9]*Space Physics Research Lab., University of Michigan, Ann Arbor, MI 48109-2143, USA*
[10]*Max-Planck-Institut für Sonnensystemforschung, D-37191 Katlenburg-Lindau, Germany*
[11]*Space Science Lab., University of California in Berkeley, Berkeley, CA 94720-7450, USA*
[12]*Space Technology Ltd., National University of Ireland, Maynooth, Co. Kildare, Ireland*
[13]*Instituto di Fisica dello Spazio Interplanetari, I-00133 Rome, Italy*
[14]*Applied Physics Laboratory, Johns Hopkins University, Laurel, MD 20723-6099, USA*
[15]*University of Bern, Physikalisches Institut, CH-3012 Bern, Switzerland*
(*Author for correspondence: E-mail: rickard.lundin@irf.se)

Abstract. Aurora is caused by the precipitation of energetic particles into a planetary atmosphere, the light intensity being roughly proportional to the precipitating particle energy flux. From auroral research in the terrestrial magnetosphere it is known that bright auroral displays, discrete aurora, result from an enhanced energy deposition caused by downward accelerated electrons. The process is commonly referred to as the auroral acceleration process. Discrete aurora is the visual manifestation of the structuring inherent in a highly magnetized plasma. A strong magnetic field limits the transverse (to the magnetic field) mobility of charged particles, effectively guiding the particle energy flux along magnetic field lines.

The typical, slanted arc structure of the Earth's discrete aurora not only visualizes the inclination of the Earth's magnetic field, but also illustrates the confinement of the auroral acceleration process. The terrestrial magnetic field guides and confines the acceleration processes such that the preferred acceleration of particles is frequently along the magnetic field lines. Field-aligned plasma acceleration is therefore also the signature of strongly magnetized plasma.

This paper discusses plasma acceleration characteristics in the night-side cavity of Mars. The acceleration is typical for strongly magnetized plasmas – field-aligned acceleration of ions and electrons. The observations map to regions at Mars of what appears to be sufficient magnetization to support magnetic field-aligned plasma acceleration – the localized crustal magnetizations at Mars (Acuña *et al.*, 1999). Our findings are based on data from the ASPERA-3 experiment on ESA's Mars Express, covering 57 orbits traversing the night-side/eclipse of Mars. There are indeed strong similarities

between Mars and the Earth regarding the accelerated electron and ion distributions. Specifically acceleration above Mars near local midnight and acceleration above discrete aurora at the Earth – characterized by nearly monoenergetic downgoing electrons in conjunction with nearly monoenergetic upgoing ions. We describe a number of characteristic features in the accelerated plasma: The "inverted V" energy-time distribution, beam vs temperature distribution, altitude distribution, local time distribution and connection with magnetic anomalies. We also compute the electron energy flux and find that the energy flux is sufficient to cause weak to medium strong (up to several tens of kR 557.7 nm emissions) aurora at Mars.

Monoenergetic counterstreaming accelerated ions and electrons is the signature of field-aligned electric currents and electric field acceleration. The topic is reasonably well understood in terrestrial magnetospheric physics, although some controversy still remains on details and the cause-effect relationships. We present a potential cause-effect relationship leading to auroral plasma acceleration in the nightside cavity of Mars – the downward acceleration of electrons supposedly manifesting itself as discrete aurora above Mars.

1. Introduction

The magnetized planets in our solar system, such as Earth, Jupiter and Saturn, are all known to accommodate aurora in their magnetic circumpolar regions. The existence of a strong planetary magnetic dipole appears to be the main condition for the occurrence of aurora, whether caused by an external/solar (e.g. the Earth) or internal (e.g. Jupiter) energy source. The distinguishing difference between "aurora" and airglow lies not in the physical atomic/molecular exitation processes, but rather in their macroscopic/structural appearance. In essence aurora may be defined as light emissions occurring within strongly magnetized plasmas. Aurora is highly structured light emissions, while airglow represents diffuse emissions.

The Earth's polar aurora and its related ionospheric and magnetospheric phenomena, is well explored and reasonably well understood. The first measurements establishing its relation with charged particle precipitation into the Earth's atmosphere was made in the early 1960s (MacIlwain, 1960). Intense aurora in the form of extended bright arcs in the sky, sometimes referred to as discrete aurora, results from downward electron acceleration at higher altitudes above the Earth. Hannes Alfvén proposed already in 1958, that magnetic field-aligned quasi-static electric fields should be an important acceleration process related with bright aurora. Field-aligned electric fields, accelerating electrons downward, will both increase the electron energy and enhance the downward electron fluxes leading to brightened auroral displays in the topside atmosphere. The first evidence for electrostatic acceleration came from sounding rockets measurements (Albert, 1967; Evans, 1968). They showed that intense fluxes of nearly monoenergetic precipitating electrons were present above auroral arcs. Subsequent low-altitude satellite measurements (Frank and Ackerson, 1971) provided a global view of the electron precipitation, demonstrating that nearly monoenergetic electron structures denoted "inverted V's"

were a common feature above the auroral oval. The notion "inverted V" referred to the spectral shape in an energy-time spectrogram. A connection between "inverted V's" and electric fields (Gurnett and Frank, 1973) supported the hypothesis of electron acceleration in an electrostatic potential structure. Evans (1974) analyzed the distribution of accelerated electrons below a field-aligned electrostatic potential, considering in detail the interaction between accelerated primary electrons and the atmosphere. The interaction leads to electron energy spectra above the aurora that contain primary/accelerated electrons as well as backscattered electrons (degraded primary- and secondary electrons).

A consequence of electrostatic acceleration is the separation of charges. If electrons are accelerated downward one expects positive ions to be accelerated upward. Indeed, narrowly collimated upward beams of accelerated ionospheric ions were eventually observed (Shelley *et al.*, 1976) at high-altitudes (4000–8000 km) above the aurora, results subsequently reconfirmed by several auroral satellites (see Moore *et al.*, 1999 for a review). Simultaneous upward accelerated ion beams and downward accelerated electron beams are therefore evidence for quasi-electrostatic acceleration of plasma along magnetic field lines.

Field-aligned electrostatic acceleration is generally discussed in connection with dipole magnetic field geometries, such as that of the Earth. Electrostatic acceleration is not expected to occur in weakly magnetized plasma environments such as those near comets, Venus and Mars. The Mars Global Surveyor (MGS) findings of strong crustal anomalies at Mars (Acuña *et al.*, 1999) have considerably changed the picture. We now expect to find diverging magnetic field "cusps" above Mars (Krymskii *et al.*, 2002) and "minimagnetospheres" (Mitchell *et al.*, 2001) with local magnetic conditions similar to those found above the Earth's polar region. A distinctive difference, though, is that the crustal magnetization is very weak compared to the Earth's dipole field. It was therefore not obvious that the plasma would be sufficiently magnetized to accommodate processes known to us from the Earth as being associated with aurora. Furthermore, the crustal field is characterized by a set of multipoles centered at specific longitudes and latitudes near the equator of Mars. The aurora, if existent, was therefore expected to be highly dependent on local time, visible only near the equatorial nightside at specific longitudes and latitudes.

The first evidence for structured emissions that could be aurora on Mars was indeed related with a crustal magnetization at Mars (Bertaux *et al.*, 2005). They also inferred the emissions to be related with particle precipitation. Publications of ongoing work followed and we now have ample evidence that intense electron precipitation occurs over magnetized regions at Mars (Lundin *et al.*, 2006a; Brain *et al.*, 2006). Evidence from ASPERA-3 data (Lundin *et al.*, 2006a) showed the signature of field-aligned plasma acceleration that suggests the existence of parallel electric field acceleration – accelerating electrons downward and ions upward. The acceleration regions, "inverted V's", are connected to semi-open flux tubes (cusps/clefts) associated with crustal magnetization regions. The latter might have been proof for a strongly magnetized plasma, if it wasn't for the lack of magnetic

field measurements on Mars Express. However, Brain *et al*. (2006a) found field-aligned currents, up to 1 microamp per square meter, associated with accelerated electrons, another signature associated with magnetic field-aligned plasma acceleration in a "strongly" magnetized plasma. Therefore, we have ample evidence for two important aspects:

1. Aurora occurs on the nightside of Mars – connected with crustal magnetization regions.
2. Auroral plasma acceleration, usually reserved for strongly magnetized planets with dipole fields, may also occur in localized magnetic cusps/clefts extending into space from weakly magnetized planets such as Mars. A solar wind / boundary layer driven generator/dynamo feeds energy to the plasma accelerator and the planetary ionosphere via field-aligned electric currents.

In this study we expand on the results of Lundin *et al*. (2006a), going into more detail on the acceleration process, its latitude and local time dependence, its altitude dependence and the energy flux expected in the nightside of Mars leading to what one may term the *aurora equatorialis*. The reason for its location so close to local midnight will be discussed. Finally, we suggest a simple concept of a current circuit that couples to the energy source – the dynamo propelled by solar wind forcing. We also discuss where and how the indirect forcing is coupled to the accelerator/load, in and above the nightside ionosphere of Mars.

2. ASPERA-3 Results

The ASPERA-3 experiment (Barabash *et al*., 2004) has two plasma instruments, an ELectron Spectrometer (ELS) and an Ion Mass Analyzer (IMA). ELS provides electron measurements in the energy range 0.001–20 keV with 8% energy resolution. The intrinsic field of view is $4 \times 360°$. The 360° aperture is divided into 16 sectors. The sensor consists of a top hat electrostatic analyzer in a very compact design.

IMA is an improved version of the ion mass spectrographs TICS/Freja, IMIS/Mars-96, IMI/Planet-B, and almost identical to the Ion Composition Analyzer, ICA, (Nilsson *et al*., 2006) on ESAs Rosetta mission. IMA provides ion measurements in the energy range 0.01–30 keV/e for the main ion components H^+, He^{++}, He^+, O^+, and the group of molecular ions ($20 < M/q < \sim 80$). IMA has a $4.6 \times 360°$ field of view. Electrostatic sweeping provides elevation ($\pm 45°$) coverage for a total field of view of about 2π. The elevation sweep shows up as periodic "pulses" in the ion energy-time spectrogram (FigureS 2 and 9).

The total material forming the basis of this study comprises over 130 orbits of ASPERA-3 data during 2004 and 2005, where we have analyzed in detail data from 57 traversals of the Martian mid-tail eclipse. During this period the spacecraft traversed the midnight sector close to the central tail. An important reason for
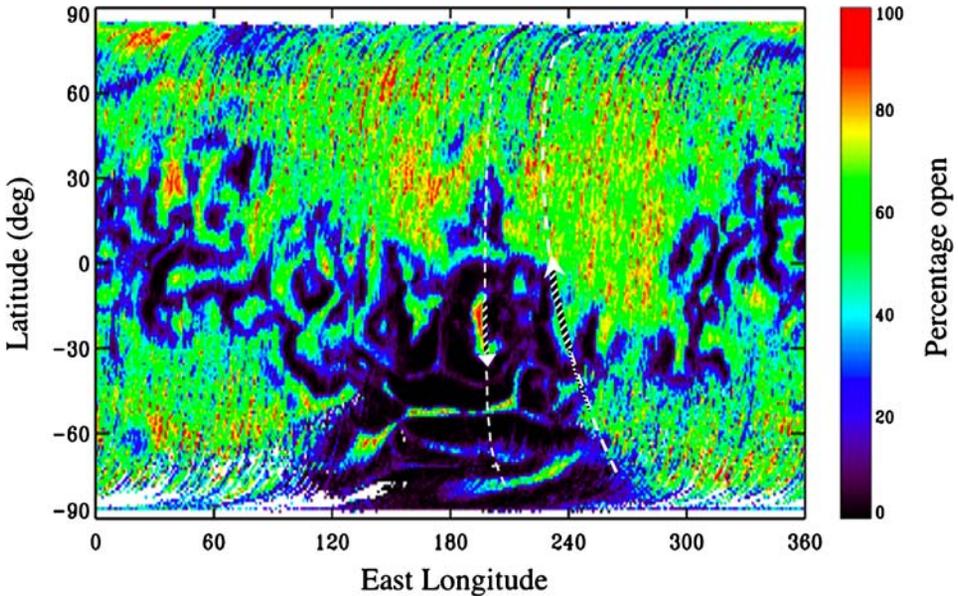
Figure 1. Nightside map of magnetic anomalies. The scale indicates the percentage of open magnetic field lines at MGS altitudes (≈400 km), red indicating 100% open and black fully closed magnetic flux tubes (after Brain *et al*., 2005). Two satellite ground tracks are marked by white dashed lines, black- and white part corresponding to the "inverted V" cases of Figure 2 (right) and 3 (left) respectively. Arrows marks the spacecraft track of the inverted V traversal.

selecting these periods was that they were characterized by coincident energization of ions and electrons in eclipse. In a number of traversals we find that the tail cavity represents a void of particles. These are all cases when the eclipse contained no passes over magnetic anomalies. In the statistics of acceleration structures presented we note that eclipses frequently contain even longer periods without-, than with plasma acceleration. There is a general lack of plasma acceleration when the spacecraft traverse regions of fully "closed" or fully open magnetic field lines (Lundin *et al*., 2006a; Brain *et al*., 2006).

Eclipse cavity passes facilitates a direct geographic mapping along magnetic field lines connecting to the magnetic cusps/clefts at Mars. This geometry provides more radial extension of the field lines into the near Mars tail. A geographic latitude and longitude projection to the 400 km MGS open/closed magnetic field map determined by Brain *et al*. (2005) is used. Figure 1 shows such a map, with the open (red) and closed (black) magnetic field lines at 400 km color-coded. Closed field lines (black) implies shielding against penetration of low energy particles, while open field lines (red) enables direct particle access to the atmosphere of Mars. On top of this map, trajectories of the Mars Express spacecraft showing orbits from two "inverted V" cases (Figures 2 and 3) are indicated, the "inverted V" marked out by hatched lines. The right dashed line corresponds to the orbit in Figure 2 and
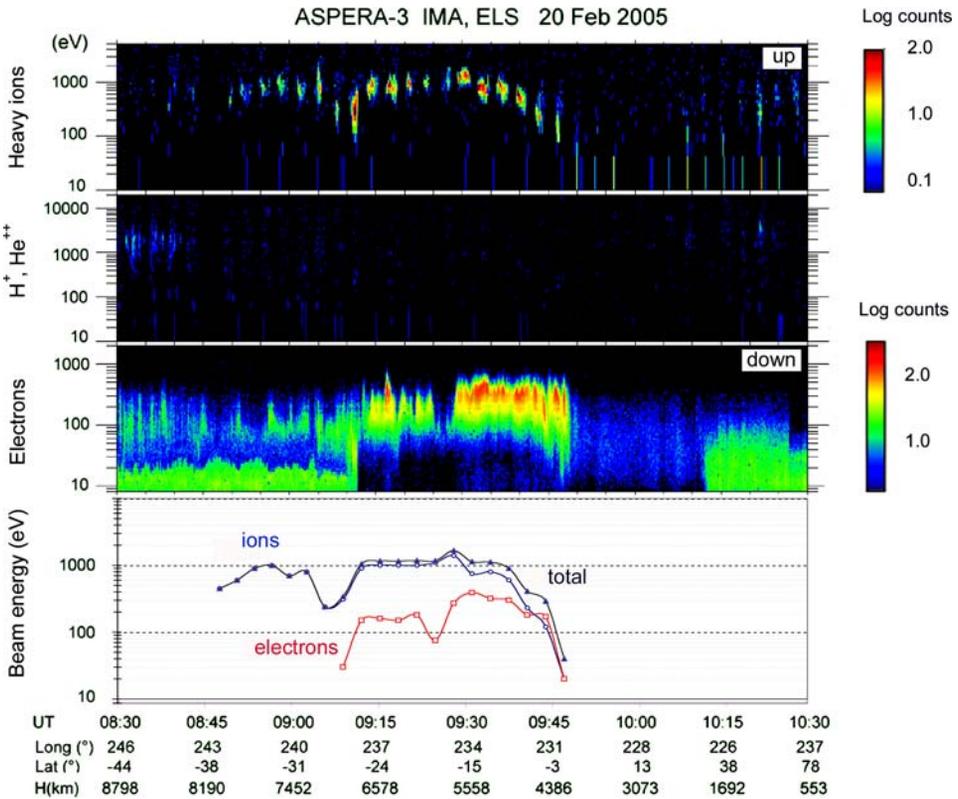
Figure 2. ASPERA-3 energy-time spectrogram and flux peak data for ions and electrons, the space-craft traversing a high-altitude "Inverted V" event in the tail-eclipse (09:13–10:12 UT). Top panel shows spectra for upgoing heavy ions (O^+, O_2^+, CO_2^+), second panel spectra for antisunward solar wind ions, and third panel spectra for downgoing electrons. The fourth panel depicts acceleration energies (peak energy) for ions (blue), electrons (red), and total acceleration (electrons + ions). The coordinates are in Mars East longitude and latitude (Figure 1).

the left hatched line passing over the "island" of open flux tubes corresponds to the orbit in Figure 3.

Figure 2 shows ion and electron energy-time spectrograms for the "inverted V" event on 20 Feb., 2005 (adapted from Lundin *et al.*, 2006a). The upper panel shows energy spectra for upgoing heavy ions using counts per readout (0.125 s). Narrow beams of heavy ionospheric ions (O^+, O_2^+, and CO_2^+) are observed flowing upward/tailward while substantial fluxes of electrons move in the opposite direction (downward/sunward). Second panel show energy spectra of solar wind ions (H^+ + He^{++}). The low/vanishing fluxes of solar wind ions demonstrate that the spacecraft was inside the induced Mars magnetosphere during this time period. The inbound and outbound crossing of IMB as determined by strong decrease/increase of sheath fluxes occurred at 08:30 UT and 10:42 UT respectively. The third panel shows energy spectra for downgoing electrons (using counts/second), the data accumulated
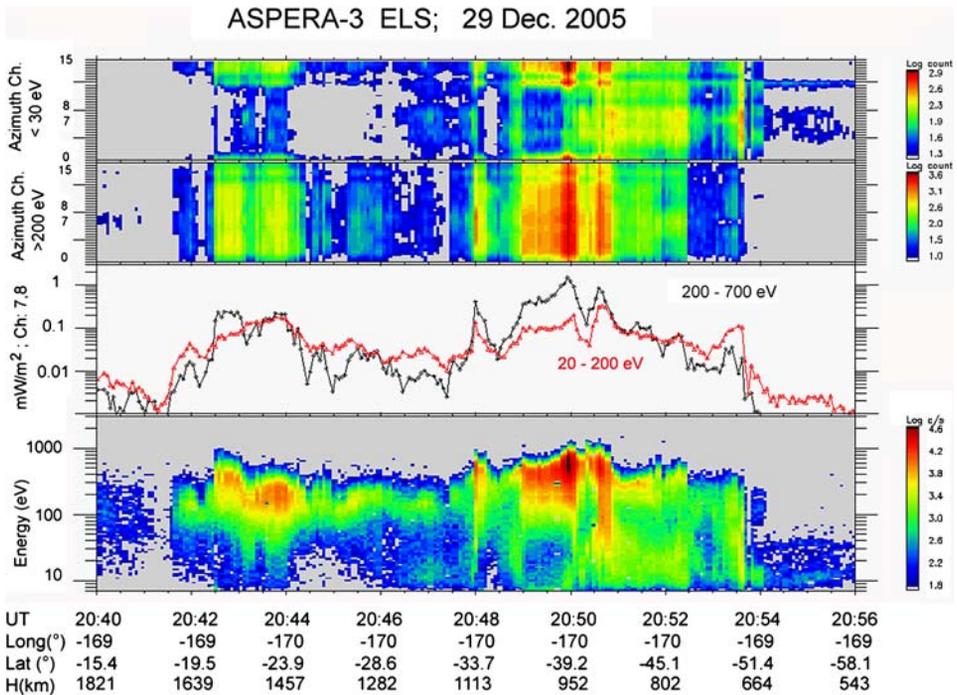
Figure 3. An example of a low-altitude "inverted V" event. The ASPERA-3 electron data is taken during a tail eclipse period (20:32–20:52 UT). The first two panels show integral counts from 16 azimuth sectors. The upper panel for <30 eV electrons, the second panels for >200 eV electrons. The third panel shows the downward energy flux (mW/m^2) in two energy intervals measured by sectors 7 and 8. Bottom panels shows energy-time spectra averaged over sectors 6–11 (downward directed). Coordinates are in Mars East longitude and latitude.

from sectors 7–10. The fourth panel shows electron and ion peak energies determined from the energy-time spectra, and the combined (total) acceleration. Notice the general characteristics of these "inverted V" events: the coincident existence of narrow upgoing ionospheric ion beams and energized downgoing electrons; the coincident acceleration of ions and electrons on what appears to be a common magnetic flux tube. This corroborates the analogy with auroral acceleration near the Earth. The MEX geographic mapping of the "inverted V" (09:10–09:50 UT) is illustrated in Figure 1. Notice that the trajectory maps to semi-open magnetic field lines – in the boundary between a magnetic anomaly and open field lines. It does not map directly to the closed flux tubes from the magnetic anomaly (dark region). This is another analogy with the Earth's auroral zone, the "inverted V's" are usually found in the boundary region between open and closed magnetic field lines.

Figure 3 shows a low-altitude "inverted V" case, this time with no data indicating ion acceleration. The energy-time spectrogram (bottom panel) is for approximately downward directed electrons (Sectors 7 and 8). The lack of observable ion fluxes

may be due to spacecraft shadow or incomplete coverage, but a more likely explanation based on the viewing direction is that the observation is made below the acceleration region. The electron energy flux peaked in this case exactly at local midnight, at an altitude of 900–1000 km above the surface of Mars. The integral downward electron energy flux corresponds to 7.0 mW/m^2. The two top panels show accumulated counts from all 16 ELS sectors for <30 eV (first) and >200 eV (second panel). The two panels illustrate the general characteristics of downward field-aligned electron acceleration, i.e. higher fluxes (counts) of electrons with energies near or above the electron peak energy (bottom panel) and enhanced fluxes of degraded primaries and backscattered electrons well below the electron peak energy.

Figure 4 shows a series of 6 ELS electron spectra taken around the region of peaked electron fluxes. The maximum peak energy, 520 eV, is at 20:49:51 UT. One immediately recognizes the typical features of the field-aligned auroral acceleration process (see e.g. Moore *et al.*, 1999 for a review). The spectral shape is evidence for "auroral" acceleration in a quasi-static electric potential drop. Based on the acceleration model by Evans, 1974 we identify three categories in the energy distribution of electrons related with downward/parallel acceleration of electrons in a potential drop V_0: the peak energy of the accelerated primaries ($E_P = eV_0$);

(1) accelerated primary electrons ($E \geq E_P$);
(2) degraded primaries and backscattered electrons ($E < E_P$);
(3) secondary electrons ($E \ll E_P$).

Degraded primaries, backscattered and secondary electrons originate from a combination of wave-particle interaction, electron back-scattering, and secondary low energy electrons emerging as a result of impacting primary electrons. The angular distribution in the downward to perpendicular direction is rather isotropic, in the sense that a downward flow is less obvious. However, this is consistent with field-aligned acceleration in a diverging magnetic field, some of the electrons magnetically mirroring before precipitating into the atmosphere (e.g. Chiu and Schulz, 1978). The precipitating electron flux, and the associated field-aligned electric current, is determined from the loss-cone. Lacking magnetic field measurements we are unable to determine the loss cone, but we may on basis of the low-energy fluxes infer that, at least part of the time, it was covered by sector 13. The reason for this is the enhanced fluxes of <100 eV electrons that stands out (20:49–20:50 UT) compared to the fluxes in other sectors. Our interpretation is that these are backscattered secondary electrons produced by energetic electron precipitation into the atmosphere of Mars (category 3)).

It is evident from Figure 4 that the peak electron energy is higher than the thermal energy of the accelerated electrons. Lundin *et al.* (2006a,b) discussed this observational fact for both ions and electrons in the eclipse cavity of Mars. Figure 5 shows an updated version of the observations by Lundin *et al.* (2006b), i.e. the relation between ion and electron beam energy versus beam temperature, respectively.
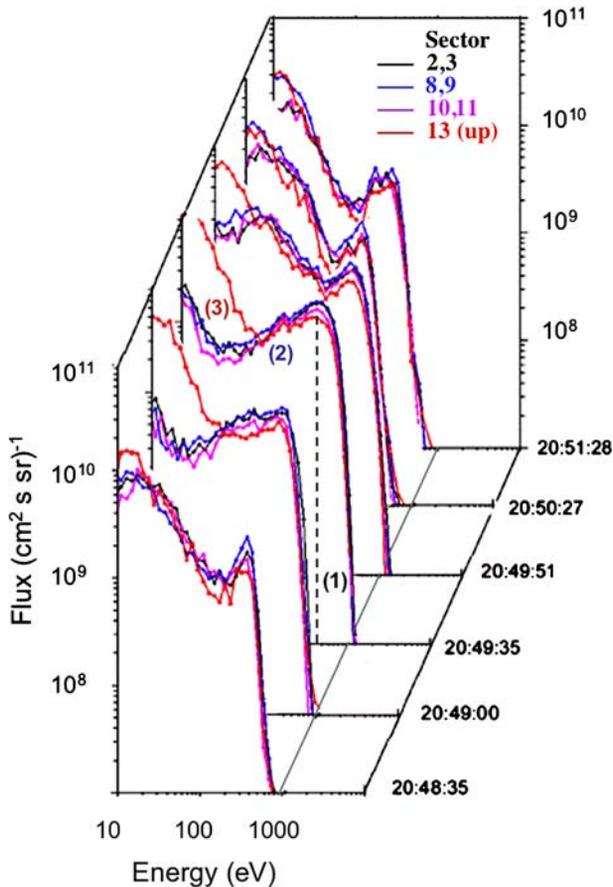
ASPERA-3 ELS; 29 Dec. 2005

Figure 4. ASPERA-3; ELS electron energy spectra taken from the low-altitude "inverted V" of Figure 3. The spectra shows the typical characteristics of field-aligned acceleration of a primary distribution (1) and the degraded primary (2) + secondary (3) electron distribution below the peak energy. The spectra are for look directions 3+4 (black), 8+9 (blue), 10+11 (magenta), and 13 (red), the latter corresponding to upgoing electrons.

Figure 5 demonstrates a good correlation between ion beam energy and ion beam temperature. The linear relation $y = 8.5x + 623$ (eV) has a correlation coefficient of 0.76. Studies of upward flowing H^+ ions, near the Earth, by the Viking satellite (Moore *et al.*, 1999; Figure 2.28) gives a linear relation $y = 4.9x + 210$ (eV) with a correlation coefficient 0.74. The relations illustrate the coupling between parallel acceleration and ion heating, with low heating rate for low parallel ion acceleration. The ion beams are cool below ≈ 1 keV, the temperature increasing proportional to the parallel energy above ≈ 1 keV, but the beam energy remain at least a factor of 10 higher than the beam temperature. In analogy with the Earth, the increased ion
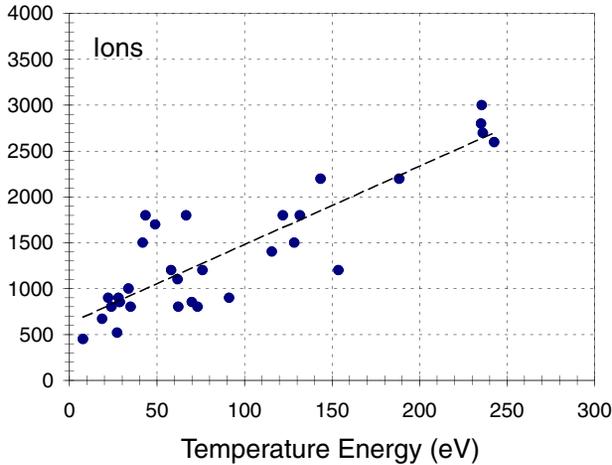
Figure 5. Ion "inverted V" peak energy versus temperature in the nightside of Mars. Oblique line marks a linear fit with function $y = 8.5x + 623$ (eV). Correlation coefficient $= 0.76$.

beam temperature may be due to a transverse (to the magnetic field) acceleration process (Sharp *et al.*, 1977). Transverse acceleration/heating are governed by a multitude of wave-particle energization processes above the Earth's polar region (Moore *et al.*, 1999). The ion acceleration as implied from Figure 5 may be due to a combined/bimodal (transverse + parallel) acceleration of ions parallel and perpendicular to the local magnetic field as suggested by Klumpar *et al.* (1984). The result of a bimodal acceleration is that the ion beam energy depends on ion mass. This fact was discovered from mid-altitude orbiting auroral satellites already in the early 1980s (Collins *et al.*, 1981). Lundin and Hultqvist (1989) presented a concept for a combined field-aligned electrostatic acceleration and low frequency wave acceleration that could explain the mass-dependent, bimodal, acceleration. They noted that low-frequency waves interacting with plasma in a diverging magnetic field leads to a velocity dependent forcing denoted "magnetic moment pumping", MMP. Guglielmi and Lundin (1999) provided a theoretical background for ponderomotive acceleration, including MMP, induced by Alfvén waves and/or ion cyclotron waves. A combination of ponderomotive forcing (MMP) and electrostatic acceleration will lead to an essentially electrostatic acceleration for electrons and a combined electrostatic and velocity-dependent (wave-induced) parallel acceleration of ions.

The ion mass-energy distribution shown in Figure 6 illustrates the mass-dependent energization of upgoing ions from Feb 20, 2005 (Figure 1). The ion mix in the beam was $47\pm10\%$ O_2^+, $37\pm8\%$ O^+, and $16\pm3\%$ CO_2^+. The average peak energy during the time interval is: $O_2^+ \approx 0.93$ keV, $O^+ \approx 0.62$ keV and $CO_2^+ \approx 1.16$ keV, suggesting a mass dependent energization process. From $v = \sqrt{2E/Nm_p}$, where N represents the number of nucleons, we find $v(O^+) \approx 85$ km/s, $v(O_2^+) \approx 71$ km/s and
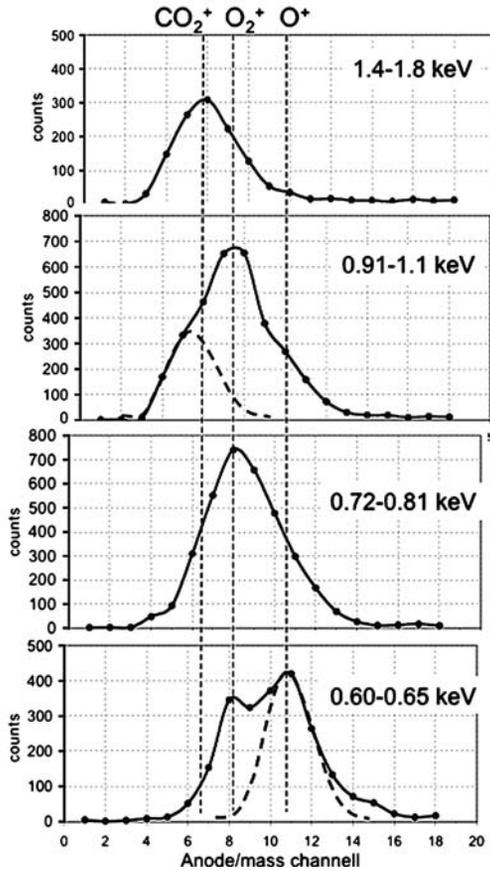
Figure 6. Ion mass spectra for 4 energy intervals for the ion beams in Figure 1, integrated over the time 09:15–09:45. Dotted lines mark the three major heavy ion species. Dashed lines shows the response for a single ion species. The average composition for the time interval is O_2^+ −49%, O^+ − 30%, and CO_2^+ −21%. Average peak energy: O_2^+ ≈0.93 keV, O^+ − ≈0.62 keV and CO_2^+ − 1.16 keV.

$v(CO_2^+) \approx 67$ km/s. These values are quite close, indicating a velocity dependent component of the field-aligned acceleration process.

Assuming now a bimodal acceleration mechanism providing an energy dependent (electrostatic) as well as velocity dependent energization we may use:

$$E = E_i + eV_0 + \frac{N m_p v_x^2}{2} \tag{1}$$

where E_i is the particle initial energy, V_0 the (electrostatic) acceleration voltage, N is the number of nucleons, m_p is the proton mass, and v_x is the velocity increase from a velocity-dependent acceleration.

Assuming that the initial particle energy is zero, the equation can be solved by making at least two simultaneous measurements for two different ions species, assuming that both species are affected by the same acceleration voltage V_0. From the energy E_1 and E_2 for the two ion species, having the number of nucleons N_1 and N_2, we get:

$$eV_0 = \frac{N_1 E_2 - N_2 E_1}{N_1 - N_2} \tag{2}$$

Taking the peak energies for O_2^+, O^+, and CO_2^+ and introducing their corresponding N (32, 16, 44) we obtain three solutions for eV_0. They all fall close to $eV_0 \approx 310$ eV. This implies that about half of the O^+ energization is due to a velocity increase; the remaining half is due to electrostatic acceleration (eV_0). For higher masses the ratio between velocity increase and electrostatic acceleration is even higher ($O_2^+ \Rightarrow$ about 2/3). By the same token we expect that electrons, having much lower mass than the ions, will be accelerated by primarily electrostatic acceleration.

The above relations represent useful tool to distinguish, by means of ion composition measurements, energy dependent acceleration from velocity dependent acceleration. The fact that a velocity-dependent acceleration appears may be responsible for half of the field-aligned acceleration is an interesting aspect that requires further considerations. It is important to note that the velocity dependent acceleration is directed, maintaining an order of magnitude lower temperature than the beam energy. It is a directed acceleration with minute ion heating, in agreement with MMP ponderomotive forcing by Alfvén waves (Lundin and Hultqvist, 1989; Guglielmi and Lundin, 1999). Intense low-frequency waves measured by MGS (Espley *et al.*, 2004) and MEX (Winningham *et al.*, 2006) may be the wave energy source for the observed velocity dependent acceleration. The analogy to the inflow of waves (e.g. Chaston *et al.*, 2005) and the corresponding wave energization observed above the Earth (e.g. André *et al.*, 1998) is striking.

Regarding the electron acceleration we find from Figure 7 that the electron beam energy and electron thermal energy display some (weak) correlation (correlation coefficient 0.58). In this case we have to infer an exponential fit for maximum correlation coefficient. The lower electron beam energy versus beam temperature ratio (2–5) compared to the ions is probably related with the high altitude origin of the electrons, most likely from the sheath and tail boundary layer. For low peak energies the electron temperatures are well in the range of typical magnetosheath electron temperatures (20–50 eV). The trend of increasing electron temperature with increasing beam energy implies a combined heating and field-aligned acceleration process. Electron heating is in general connected with wave activity along Terrestrial auroral field lines. Wave activity inferred from high-time resolution ELS data in connection with ion and electron acceleration (Winningham *et al.*, 2006; Lundin *et al.*, 2006b) implies similar heating processes near Mars. An ongoing study using orbit conjunctions between MGS and MEX, combining magnetic field, electron and ion data will elaborate further on this topic.
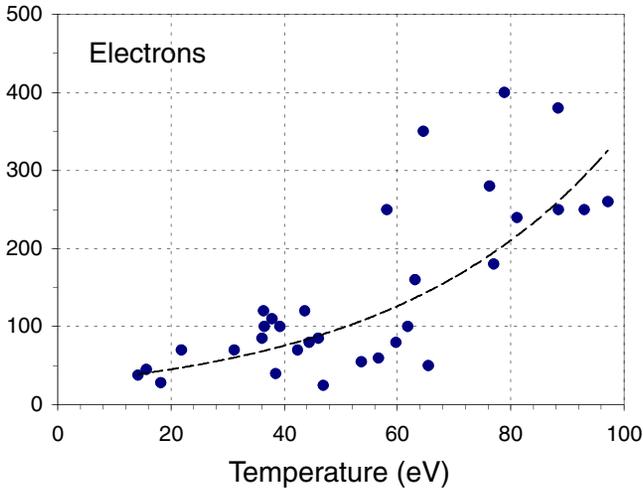
Figure 7. Electron "inverted V" peak energy versus temperature in the night-side of Mars. Dashed line marks an exponential fit with function $y = 27.2\exp(0.026x)$ (eV). Correlation coefficient $= 0.58$.

Having concluded that acceleration process affect ions and electrons slightly differently, an imminent question is where? We noted already the close connection to the crustal magnetic field in the midnight sector of Mars, so relevant issues are therefore the altitude, local time and geographic distribution.

Figure 8 shows the relative contribution of ions to the total (electron + ion) acceleration. The basis is a downward acceleration of electrons and upward acceleration of ions, the total acceleration in a flux tube given by the sum of the ion and electron acceleration. The total/maximum acceleration achievable corresponds to the ion beam energy in the tail, above the acceleration region, and the electron beam energy below the acceleration region in the upper ionosphere of Mars. This is corroborated in Figure 8. The altitude dependence suggests a gradual change/turnover of the acceleration, the acceleration taking place between the ionosphere and some 10 000 km above Mars. The figure also suggests that a large fraction of the acceleration takes place at altitudes below 2000 km.

The relative contribution of ion acceleration to the total acceleration (ion acceleration/total acceleration), support the hypothesis that the acceleration is at least in part due to altitude dependent electric field acceleration. Dashed line gives a logarithmic fit to the data points, the correlation coefficient being $R^2 = 0.78$. The logarithmic fit gave in fact the best correlation of all fits. The lack of accelerated electrons observed above $\approx$8000 km implies a height limited process. This is expected if the acceleration process is coupled to the crustal magnetic field at Mars. The confined regions of crustal magnetization imply a rapid decrease of the magnetic field intensity with height, but the field lines may yet extend far into the tail of the Martian umbra.
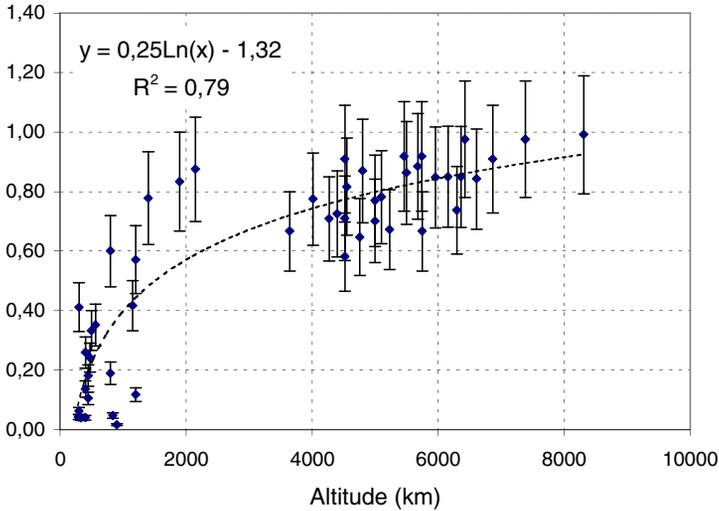
Figure 8. Relative ion contribution to the total acceleration versus altitude. Dashed curve shows a logarithmic fit to the data with correlation coefficient 0.79. Error bars marks estimated errors in determining the relative ion contribution of the total ion+electron acceleration.

While Figure 8 illustrates a statistical/average situation, Figure 9 shows a case of the instantaneous coupling between ion and electron acceleration, i.e. the ion acceleration decreases simultaneously with an increase of the electron acceleration. The total/average acceleration stays rather constant, indicating that the spacecraft encounters a gradient of the acceleration region, where the downward acceleration of electrons briefly extends to higher altitudes. In analogy with field-aligned electrostatic acceleration over the Earth's auroral oval, one may envisage this case as an apparent dip towards the center of the field-aligned electric field region. Notice that the electrons display a similar variability versus energy as that observed in Figures 2 and 3, again suggesting a simultaneously operating wave induced velocity dependent acceleration.

The final issue concerns the mapping of nightside/eclipse plasma acceleration to Martian magnetic anomalies. Figure 10 shows a projection of the 57 "inverted V" cases in solar ecliptic latitude and longitude. There is a clear tendency for "inverted V's" to occur near local midnight, the observations clustering around an average local time, latitude entry (LT = 23.1, lat = −5.3°) and exit (LT = 23.4, lat = −11.3°) of the "inverted V's". The clustering of observations close to local midnight is in part due to the selection criteria (eclipses), but it can neither explain the clear shift of the encounters towards the evening sector, nor can it explain the strong clustering within three hours of local midnight.

In Figure 11 we have instead plotted the "inverted V" footprints versus geographic latitude and longitude. This provides a more dispersed picture compared to Figure 10. Notice that we have transformed the background map (Figure 1) such
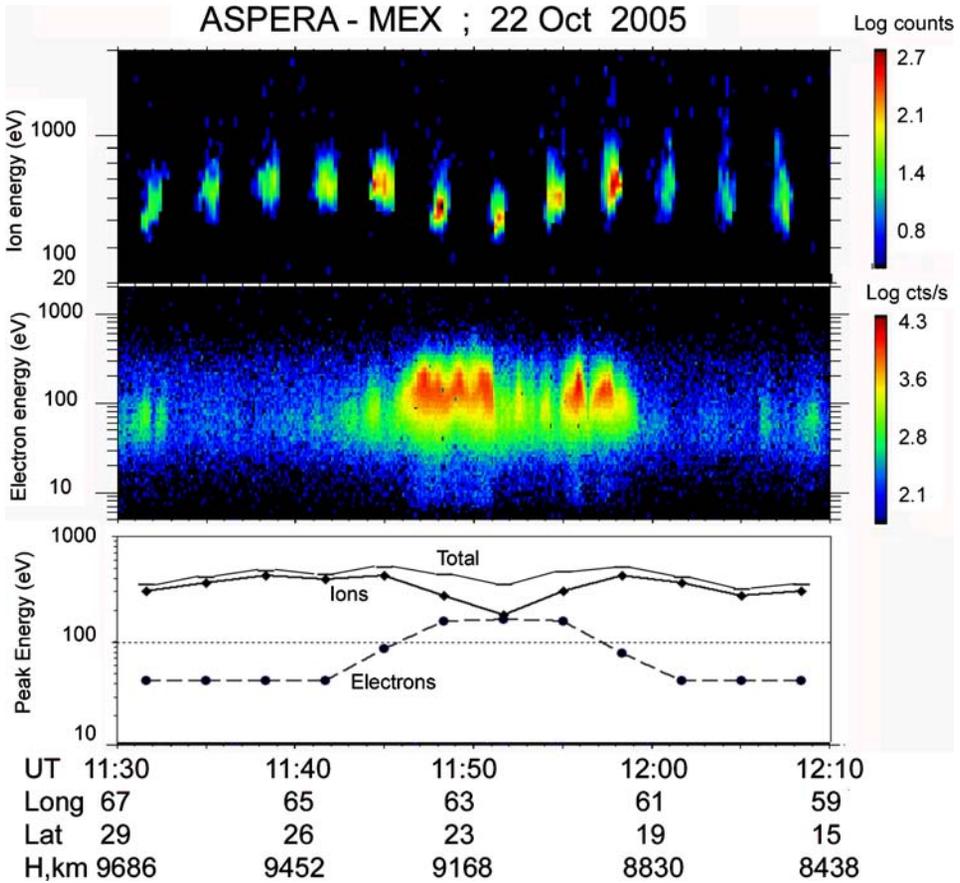
Figure 9. Energy time spectra for upgoing ions (upper panel) and downgoing electrons (middle panel) in the acceleration region. The bottom panel shows peak energies for ions, electrons, and sum peak energy (ions-electron). The event illustrates the strong coupling between electron and ion acceleration.

that the extremes – open field lines and closed field lines, are colored black. White lines mark the latitude and longitude mapping of the "inverted V's" above Mars. Clearly there is a clustering of data points in transition regions between open and closed field lines. Few data points fall within larger areas of open (black) or closed (black) magnetic field lines. We therefore conclude that the "inverted V's" are associated with boundary regions between open and closed field lines. The precipitation of electrons and the corresponding acceleration and escape of ionospheric ions appear to take place in either cusps interfacing magnetic anomalies or near the outer boundary interfacing the large-scale magnetic anomaly region with the non-magnetized region of Mars.

To complete the analogy between Terrestrial discrete aurora and Martian aurora the local downward energy flux of electrons is determined as well as the
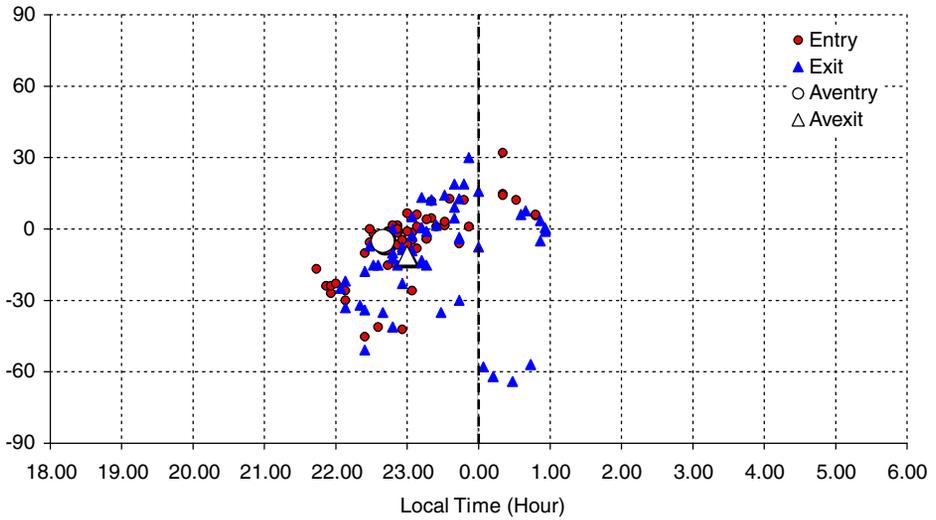
Figure 10. The distribution of nightside ion "inverted V's" plotted versus solar ecliptic (SE) coordinates. Notice the agglomeration of data points near local midnight. Entry and exit of the "inverted V's" are marked by different symbols. Average entry (LT = 23.1, lat = −5.3°) and exit (LT = 23.4, lat = −11.3°) are also marked.
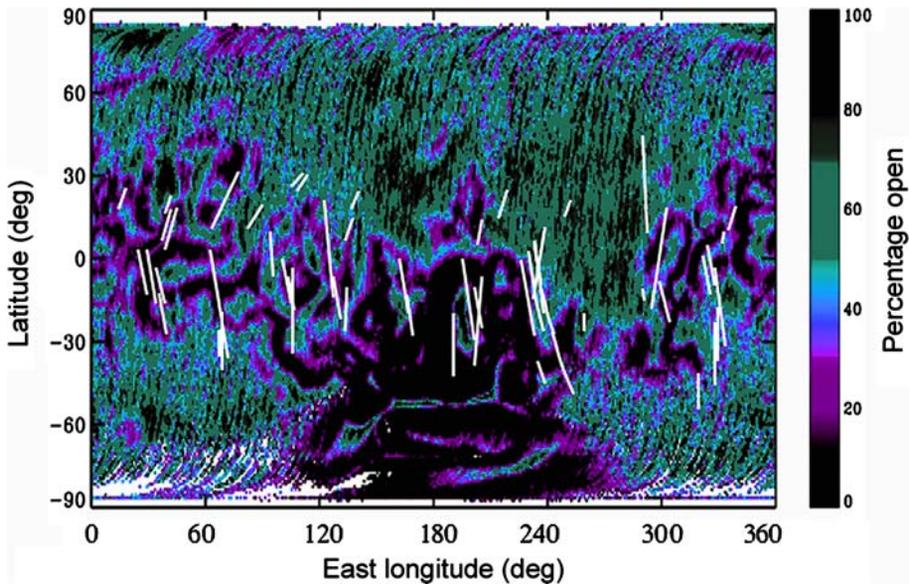

Figure 11. Ground track projections of nightside ion "inverted V's" and their relation to the percentage of open field lines over crustal magnetic regions at Mars.

electron energy flux expected on top of the atmosphere from the acceleration of electrons below the spacecraft. The latter was computed using the acceleration voltage (eV_0) inferred from the almost monoenergetic outflowing ionospheric ion beams (Figures 1 and 5). As noted from Equations (1, 2) and the related text, ponderomotive acceleration by waves may correspond to about half of the ion acceleration. Therefore, a much more detailed analysis is required to infer correctly the electrostatic part of the field-aligned acceleration. Nevertheless, we will here for the sake of simplicity assume that the ion and electron acceleration is not mass (velocity) dependent, enabling an "electrostatic scaling" as described below. The assumption is quite reasonable considering the finding in Figure 9, i.e. the electron and ion peak energy scales almost equally. For electrostatic acceleration along a unit magnetic flux tube the total energy flux gain is given by:

$$P_a = \left(\frac{B_a}{B_i}\right) eV_o \Phi_i \tag{3}$$

where Φ_i represents the local downward electron flux, V_0 the acceleration voltage, and B_a/B_i is the ratio of the magnetic field along the accelerating flux tube, the subscript a marking top of atmosphere (also bottom of acceleration structure) and subscript i marking the locus of observation above eV_0. Assuming for the sake of simplicity that the acceleration takes place in a narrow altitude region ($B_a/B_i \approx 1$) we obtain: $P_a \approx eV_o \Phi_i$, i.e. the downward electron energy flux above the atmosphere is given by:

$$\Theta_a = \Theta_i + eV_0 \Phi_i \tag{4}$$

where Θ_i is the locally measured downward electron energy flux. In Figure 12 we have plotted Θ_a versus Θ_i for 28 different cases. We note here that the locally measured energy flux is in the range 0.01–$10\,\mathrm{mW/m^2}$ while the accelerated precipitating energy flux into the upper nightside atmosphere of Mars is in the range 1–$25\,\mathrm{mW/m^2}$. The latter is indeed a substantial electron precipitation, the highest value corresponding to rather bright aurora at the Earth ($\approx 40\,\mathrm{kR}$ of $557.7\,\mathrm{nm}$). The naked eye catches an aurora in the range a few kR in full darkness, and the aurora stands out clearly above $10\,\mathrm{kR}$. The auroral light is produced from excitation of atoms and molecules in the upper atmosphere, the lines reflecting the composition of the gas. The auroral light intensity is related to how emission lines are stimulated by particle precipitation, the emissions discovered in 150–$300\,\mathrm{nm}$ band (CO and O) by Bertaux *et al.* (2005) being less referred to in connection with terrestrial aurora. More data about the upper atmosphere composition is therefore needed to make a more detailed comparison between Martian and Terrestrial aurora.
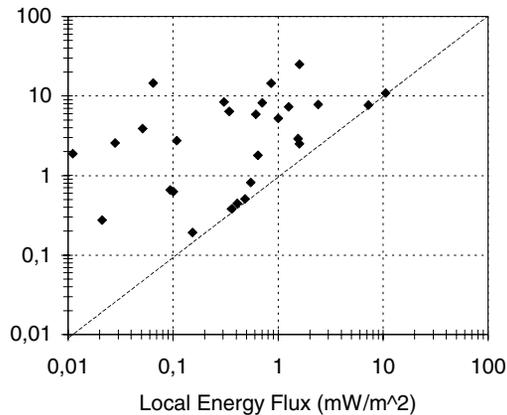
Figure 12. In-situ measured electron energy flux plotted versus model energy flux determined from
an electrostatic parallel acceleration below the s/c. Low-altitude acceleration (eV_0) is determined by
the peak energy of upgoing ion beams. The diagonal line, indicating no acceleration below the s/c,
shows that parallel acceleration amplifies the downward energy flux by of the order a factor of ten.
Measurements points falling along the diagonal line were all taken at altitudes below 900 km.

3. Discussions and Conclusions

Plasma acceleration with "inverted V" like ion features have been reported from the
Phobos-2 spacecraft orbiting Mars (Lundin *et al.*, 1989) and more recently by Mars
Express (Lundin *et al.*, 2006a,b). A connection with aurora, and the corresponding
auroral plasma acceleration process, could be made following the discovery of
localized strong magnetization regions in the Martian crust (Acuna *et al.*, 1999).
This lead to speculations about magnetic topologies and ionosphere processes above
Mars similar to those above the Earth (e.g. Mitchell *et al.*, 2001; Krymskii *et al.*,
2002). It also lead to experiments pinpointing towards the interesting magnetic field
regions and to the identification of auroral-like emissions (Bertaux *et al.*, 2005) and
the occurrence of auroral acceleration process in regions connected to the crustal
magnetic field at Mars (Lundin *et al.*, 2006a).

  The plasma acceleration leads to an inflow of external (solar wind) plasma as
well as an outflow of ionospheric plasma at Mars. Both inflow and outflow lead to
losses, the inflow (of energetic electrons) causing ionization in the nightside upper
atmosphere, thereby promoting plasma acceleration and escape. While ionospheric
plasma losses are effective on the solar EUV illuminated dayside exposed to a
fierce bombardment of solar wind plasma (e.g. Perez-de Tejada, 1987; Lundin
et al., 1989; Luhmann and Bauer, 1992), it is supposedly less effective in the deep
nightside of Mars. Direct nightside losses will require processes in the tail cavity
that can channel energy down to the (tenuous) nightside ionosphere.

  Results from ASPERA-3 on MEX (Lundin *et al.*, 2004) suggest that energization
and outflow of plasma may initiate at fairly low altitudes, on the dayside potentially

below the MEX pericenter ($\approx$270 km). Similarly, the nightside energization and outflow may also reach down to low altitudes, perhaps even lower in view of the low nightside ionization rate.

The auroral acceleration process is usually connected with strongly magnetized plasmas interacting with a planetary ionosphere, such as the hot plasma contained in the magnetospheres of Earth, Jupiter and Saturn. It is therefore not an obvious case for Mars. The solar wind interaction with Mars is essentially Venus like or comet like, the crustal magnetic field regions mainly perturbing the solar wind interaction with Mars. However, the process evidently operates in the tail shadow zone of Mars where the field lines from the crustal magnetizations may extend out and contain sufficiently tenuous plasma. The latter enables stronger magnetic control, leading to morphologies and an ionosphere-magnetosphere interaction that resembles that taking place in the Earth's distant magnetotail. Besides commonalities presented here between the Earth's auroral plasma acceleration and the accelerated plasma in the nightside cavity of Mars, the findings by Brain *et al.* (2006a) adds another aspect into this – the field-aligned electric currents (FACs, Iijima and Potemra, 1976). It is well known from the terrestrial magnetospheric physics that FACs play an important role in the magnetosphere-ionosphere interaction (see e.g. Moore *et al.*, 1999). The FACs are connected to the ionosphere (load) in one end and to a dynamo/generator in the other. In this way the interaction may be described by a simple electric current circuit analogy. The interaction is in reality much more complex, involving waves, current limitations and instabilities etc. However, the electric current circuit analogy is yet an important aid into understanding the cause-effect relationship.

Figure 13 is a diagrammatic representation of a dynamo driven current circuit connecting to the nightside ionosphere at Mars. The upper panel is a view perpendicular to the ecliptic plane showing how solar wind plasma forcing sets up a dynamo, producing transverse/dynamo currents ($\underline{j} \times \underline{B} = \nabla \underline{P} > 0$) closing in the ionosphere (load) via FACs. The field-aligned potential drop on the negatively polarized side of the dynamo (lower panel) acts as an accelerator for particles, upward for ions and downward for electrons. Downward accelerated electrons represent the energy source for the aurora. The dynamo itself is governed by the external solar wind forcing, i.e. as long as a plasma dynamic pressure gradient ($\nabla \underline{P}$) can be maintained perpendicular to B. That situation is quite unstable, though, in view of the geometrical constraints of a magnetic flux tube attached to the surface at Mars in a relatively confined region. A "flapping" oscillatory motion may be induced by the external flow, the dynamic pressure gradient varying with the eigenfrequency of the flux tube. The corresponding acceleration of electrons may vary with the frequency of a standing Alfvén wave. Such variable signatures are in fact observed in the accelerated electron distribution. Notice for instance in Figures 2 and 9 that the electron energy peaks are modulated with a periodicity ranging between 1–2 min.

In this report we have analyzed in more detail the auroral acceleration process in the nightside/eclipse of Mars above magnetic anomalies (Lundin *et al.*, 2006a). The observational data is extended to lower altitudes and we have elaborated on the
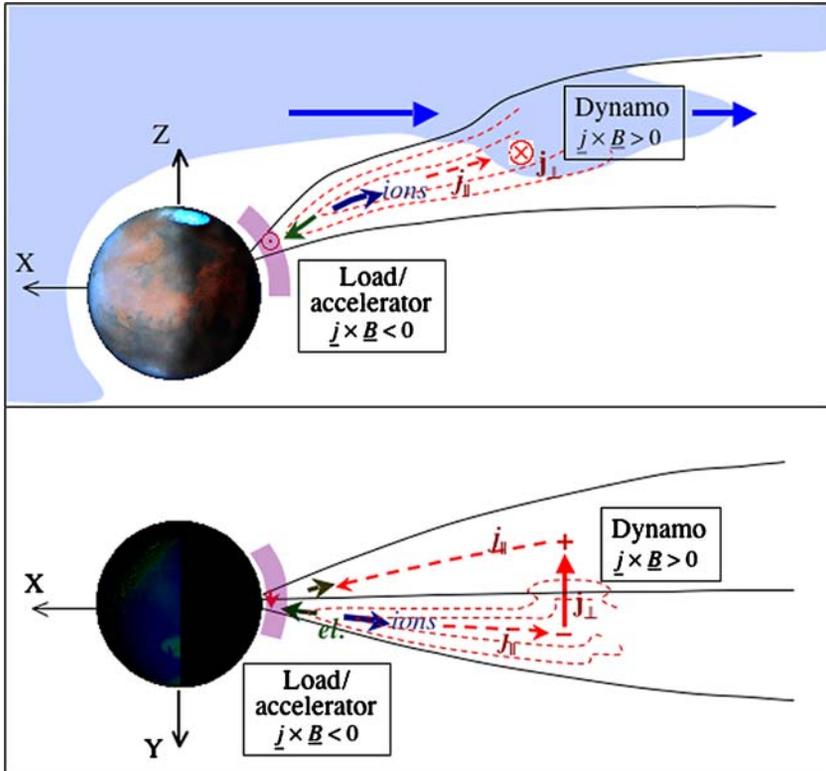
Figure 13. Diagram of the field-aligned auroral plasma acceleration region above a magnetic cusp/cleft at Mars. The dynamo is governed by the cross-field flow of solar wind plasma. The current circuit, driven by the dynamo, consists of a pair of field-aligned currents and an ionospheric closure current.

potential energy source, the dynamo driving the auroral acceleration process above Mars. The energy and mass sources are aspects of the dynamo-accelerator that requires further studies. The outflowing ions clearly originate from the ionosphere. On the other hand the high altitude source, the solar wind plasma access of magnetic flux tubes connected to Mars, remains an issue for future studies. The intense fluxes of upgoing ionospheric ions from a tenuous nightside ionosphere suggest the formation of auroral plasma density cavities, like in the Earth's nightside ionosphere (Calvert, 1981). A combination of parallel electric fields and waves deepens the cavity and promotes a bimodal acceleration process (e.g. Klumpar *et al.*, 1984). A combined velocity dependent and energy dependent field aligned acceleration will manifests itself as a mass-dependent acceleration process (Lundin and Hultqvist, 1989) leading to different peak energies for different masses as first reported on by Collin *et al.* (1984). Velocity dependent acceleration in a non-magnetized planetary environment is also the characteristics of a pick-up process as described Luhman

and Schwingenshuh (1990). However, we report here on nearly antisunward ion outflow extending from magnetic anomalies projected to the planetary ionosphere – at low altitudes near local midnight. Considering the draped tail magnetic field of Mars we may therefore exclude contributions from a transverse (to B) pickup process in the solar wind electric- and magnetic field. One may of course interpret the velocity-dependent part of the acceleration as an "ion pickup" process, but then in a strong diverging crustal magnetic field, similar to that in the Earth's dipole field above the auroral oval.

The overall situation in the tail umbra of Mars and the Earth therefore show a number of similarities, in particular with respect to the acceleration of plasma, eventually leading to aurora in their respective topside atmosphere. The "inverted V" electron and ion energy-time characteristics, the mass dependence of the ion acceleration, the electron energy distribution, the altitude distribution, and the close connection to the planetary magnetic field are all in support for such a conclusion. A more enigmatic feature is the concentration of events to midnight, with a significant shift towards premidnight at Mars. An external solar wind electric field forcing may in principle cause such an organization, but only if it is unidirectional and likewise for the Martian magnetic field. Anything else would lead to a spread around midnight. Another possible explanation is that the Mars rotational speed can cause a "Parker spiral" effect of the escaping ionospheric plasma. However, estimates lead to a time shift of no more than 10 minutes, while the average shift is about 1 hour. Moreover, the mapping always falls close to the "expected" crustal magnetic field regions. Thus, there is no apparent shift of the magnetic field lines towards dawn or dusk. This implies that it is the source region, the dynamo that is being shifted towards dusk. For what reason, that is the question.

References

Acuña, M. J., Connerey, J., Ness, N., Lin, R., Mitchell, D., Cralsson, C., *et al*.: 1999, *Science* **284**, 790.

Albert, R. D.: 1967, *Phys. Rev. Lett*. **18**, 368.

André, M., Norqvist, P., Andersson, L., Eliasson, L., Eriksson, A. I., Blomberg, L., *et al*.: 1998, *J. Geophys. Res*. **103**, 4199.

Barabash, S., Lundin, R., Andersson, H., *et al*.: 2004, The Analyzer of Space Plasmas and Energetic Atoms (ASPERA-3) for the Mars Express Mission, In Mars-Express – The Scientific Payload, ESA-SP-1240.

Bertaux, J.-L., Leblanc, F., Witasse, O., Quemerais, E., Lilensten, J., Stern, S.A., *et al*.: 2005, *Nature* **435**, 9.

Brain D., Luhmann, J., Mitchell, D., and Lin, R.: 2005, Expected influence of crustal magnetic fields on the ASPERA3 ELS observations: Lessons learnt from MGS. Paper presented at 1st mars Express Science conference, 21–25 Feb, 2005.

Brain, D. A., Halekas, J. S., Peticolas, L. M., Lin, R. P., Luhmann, J. G., Mitchell, D. L., *et al*.: 2006, *Geophys. Res. Lett.,* 10.1029/2005GL024782.

Calvert, W.: 1981, *Geophys. Res. Lett*. **8**, 919.

Chaston, C. C., Peticolas, L. M., Carlson, C. W., McFadden, J. P., Mozer, F., Wilber, M., *et al*.: 2005, *J. Geophys. Res.* **110**, A02211, doi:10.1029/2004JA010483.

Chiu, Y. T., and Schulz, M.: 1978, *J. Geophys. Res.* **83**, 629.

Collin, H. L., Sharp, R. D., and Shelley, E. G.: *J. Geophys. Res.* **89**, 2185.

Dubinin, E., Lundin , R., Koskinen, H., and Pissarenko, N.: 1993, *J. Geophys. Res.* **98**, 3991.

Evans, D. S.: 1968, *J. Geophys. Res.* **73**, 2315.

Evans, D. S.: 1974, *J. Geophys. Res.* **79**, 2853.

Espley, J. R., Cloutier, P. A., Crider, D. H., Brain, D. A., and Acuña, M. H.: 2004, *J. Geophys. Res.*, 2004AGUFMSA13A1120E.

Frank, L. A. and Ackerson, K. L.: 1971, *J. Geophys. Res.* **76**, 3612.

Guglielmi, A. and Lundin, R.: 2001, *J. Geophys. Res.* **106**, 13219.

Gurnett, D. A. and Frank, L. A.: *J. Geophys. Res.* **78**, 145.

Iijima, T. and Potemra, T. A.: 1976, *J. Geophys. Res.* **81**, 2165.

Kallio, E., Barabash, S., Luhmann, J. G., Koskinen, H., Lundin, R., and Norberg, O.: 1994, *Geophys. Res. Lett.* **99**, 23547.

Klumpar, D. M., Peterson, W. K., and Shelley, E. G.: 1984, *J. Geophys. Res.* **89**, 10779.

Krymskii, A. M., Breus, T. K., Ness, N. F., Acuña, M. H., Connerney, J. E. P., Crider, D. H., *et al*.: 2002, *J. Geophys. Res.* **107**(A9), 1245, doi:10.1029/2001JA000239.

Luhman, J. G. and Schwingenshuh, K.: 1990, *J. Geophys. Res.* **95**, 939.

Luhmann, J. G. and Bauer, S. J.: 1992, AGU monograph **66**, 417.

Lundin, R., Zakharov, A., Pellinen, R., Hultqvist, B., Borg, H., Dubinin, E. M., *et al*.: 1989, *Nature* **341**, 609.

Lundin, R. and Hultqvist, B.: 1989, *J. Geophys. Res.* **94**, 6665.

Lundin, R., Barabash, S., Andersson, H., Holmström, M., *et al*.: 2004, *Science* **305**, 1933.

Lundin, R., Winningham, D., Barabash, S., *et al*.: 2006a, *Science* **311**, 980.

Lundin, R., Winningham, D., Barabash, S., Frahm, R., and the ASPERA-3 team: 2006b, *ICARUS*, April 2006.

Lyons, L. R., Koskinen, H. E. J., Blake, J. B., Egeland, A., Hirahara, M., Øieroset, M., *et al*.: 1999, *Space Sci. Rev.* **88**, 85.

MacIlwain, C. E.: 1960, *J. Geophys. Res.* **65**, 2727.

Mitchell, D. L., Lin, R. P., Mazelle, C., *et al*.: 2001, *J. Geophys. Res.* **106**, 23419.

Moore, T. E., Lundin, R., Alcayde, D., Andre, M., Ganguli, S. B., Temerin, M., *et al*.: 1999, *Space Sci. Rev.* **88**.

Pérez-de Tejada, H.: 1987, *J. Geophys. Res.* **92**, 4713.

Russell, C. T., Luhmann, J. G., Schwingenshuh, K., Riedler, W., and Yeroshenko, Ye: 1990, *Geophys. Res. Lett.* **17**, 897.

Sharp, R. D., Johnson, R. G., and Shelley, E. G.: 1977, *J. Geophys. Res.* **82**, 3324.

Shelley, E. G., Johnson, R. G., and Sharp, R. D.: *Geophys. Res. Lett.* **3**, 654.

Winningham, J. D., Frahm, R. A., Sharber, J. R., Coates, A. J., Linder, D. R., Soobiah, Y., *et al*., and the Aspera-3 Team: 2006, *ICARUS*, April issue.